

STUDY OF 2D SLOT STABILIZED FLAME FOR UNPERTURBED AND PERTURBED EQUIVALENCE RATIO

*A Thesis submitted
for the degree of
Master of Engineering
in
Aerospace Engineering
by*

Dhadphale Jayesh Manohar



Department of Aerospace Engineering
Indian Institute of Science
Bangalore – 560 012 (INDIA)

August, 2017

© Dhadphale Jayesh Manohar

August 2017

All rights reserved

Dedicated

to

My Family

Acknowledgements

I would like to thank Professor Santosh Hemchandra, for his guidance and insightful discussions which helped me a lot in understanding subtle details of combustion physics. The suggestions made by him helped me to tackle problems which I faced during the project.

I am also thankful to Kiran S. for his simplified explanations regarding solver modules and help in debugging the same. I would like to thank Prasad B. and Kiran M. for their suggestions and technical support throughout the project.

I would like to thank Kiran R. for explaining grid generation in C and using solver. I also would like to thank Raghav S. and Arpit S. for their help to install CANTERA.

Finally, I would like to thank my parents and family for their support and constant encouragement.

Abstract

Flame speed is sensitive to strain rate and curvature of the flame surface. Slot stabilized flame have curvature and strain rate variation along the flame surface. Hence variation of the flame speed with this two parameters is carried out for steady unperturbed slot stabilized flame.

Local quenching of reactions on the flame surface is of serious concern in lean combustion devices which is directly related to net heat release rate and performance of the system. Steady flammability limit based extinction criterion has found to be more restrictive and demands unnecessary high equivalence ratio [11]. Sankaran and Im [11] have suggested the concept of dynamic flammability limit, so as to include effect of flow time scale(strain rate) and equivalence ratio perturbation on flammability limit.

Bansal and Im [1] have extended the concept of dynamic flammability limit. They have studied counter-flow premixed flame configuration subjected to various strain rates and has successfully incorporated various time scales in combustion to make extinction criteria more generalized. They also have proposed a Dynamic Flammability Limit Extension (DFLE) as a function of non-dimensional frequency (η).

Bansal et al. [1] work is mainly done for counter flow configuration hence its applicability to 2D slot stabilized flame is studied here.

Contents

Acknowledgements	i
Abstract	ii
Contents	iii
List of Figures	v
List of Tables	viii
1 Introduction	1
1.1 Organization of Thesis	6
2 Formulation and Computational Setup	7
2.1 Solver Description	7
2.2 Case Setup	8
2.2.1 Grid Generation	8

CONTENTS

2.2.2	Initial Condition and Boundary Conditions	8
2.2.3	Forced Case	10
3	Steady State	13
3.1	Flame Speed Calculation	13
3.2	Curvature effect on flame speed	16
3.3	Strain rate (κ) effect on Flame Speed	17
4	Perturbed Cases	22
4.1	Case: $\epsilon = 0.05$	24
4.2	Case: $\epsilon = 0.2, \epsilon = 0.4$	25
4.2.1	Extinction Analysis:	28
5	Conclusion	35
	Bibliography	36

List of Figures

1.1	<i>DFLE</i> as a function of non-dimensional frequency (η)	4
1.2	Equivalance ratio oscillation induced effects [12] (slightly modified)	5
2.1	Schematic of 2D slot stabilized flame used for present simulations	9
2.2	Mesh used for present simulations with every point in the grid (fine mesh in the flame region and stretched outside)	10
2.3	Initial conditions for Temperature and species which vary from un-burnt to burnt state across the flame.(b) Axial velocity initialized with same profile as at inlet. . .	11
3.1	Temperature field with Heat Release rate contour in black and overlapped velocity vector field	14
3.2	Steady State fields for CH_4 , CO , H_2 , H , H_2 and Heat Release rate per unit volume (\dot{H})	15
3.3	Normal to the contour of $T=350K$	16
3.4	Axial variation of $S_L(m/s)$	17
3.5	Axial variation of curvature ($C(1/m)$)	18

LIST OF FIGURES

3.6 Variation of flame speed (S_L) with curvature ($C(1/m)$)	19
3.7 Axial variation of Strain Rate ($\kappa(1/s)$)	19
3.8 Variation of flame speed (S_L) with Strain Rate ($\kappa(1/s)$)	20
3.9 Flame speed(S_L) vs strain rate(κ) with linear fit.	20
3.10 Comparison of Markstain length by Varea et al. [15] with computed L_u	21
4.1 Plot of present cases on figure 1.1	23
4.2 Comparative plots of of $(\phi - \phi_t)$, Temperature(K) fields with Hear release rate(\dot{H}) contours and velocity vector field for different phase angles at Inlet ($\bar{\phi} = 0.6$, $\epsilon = 0.05$, $f = 60Hz$)	24
4.3 Comparative plots of of $(\phi - \phi_t)$, Temperature(K), Hear Release Rate contours and velocity vector field for different phase angles at Inlet ($\bar{\phi} = 0.6$, $\epsilon = 0.2$, $f = 60Hz$)	26
4.4 Comparative plots of of $(\phi - \phi_t)$, Temperature(K), Hear Release Rate contours and velocity vector field for different phase angles at Inlet ($\bar{\phi} = 0.6$, $\epsilon = 0.4$, $f = 60Hz$)	27
4.5 Comparative plots of of $(P - P_{atm})$ and Dilatation rate(1/s) field($\bar{\phi} = 0.6$, $\epsilon = 0.4$, $f = 60Hz$)	29
4.6 Comparative plot of $\phi - \phi_t$ and Temperature(K) field with heat release rate contour(\dot{H}) for $\bar{\phi} = 0.6$, $\epsilon = 0.4$, $f = 60Hz$ case.	30
4.7 Plot of parameter β along axial direction.	31
4.8 Volumetric molar production rate of CH_4 at (a)steady state and(b) For $\epsilon = 0.4$ case, with 270° phase at inlet.	32

LIST OF FIGURES

4.9 Volumetric molar production rate of H , H_2 and OH . (a),(c),(e) show steady state and(b),(d),(f) show $\epsilon = 0.4$ case, with 270° phase at inlet.	33
4.10 Volumetric molar production rate of HO_2 at (a)steady state and(b) For $\epsilon = 0.4$ case, with 270° phase at inlet.	34

List of Tables

4.1 Normalized minimum equivalence ratio(ϕ_{min}^*) Calculation	22
--	----

Chapter 1

Introduction

Adiabatic flame speed is the fundamental quantity in combustion. It is found that flame speed is sensitive to flow field(strain rate) and flame shape(curvature). Hence experimental measurement of flame speed for flat unstrained flame is difficult. As slot stabilized flame is strained and have curvature, hence to measure flame speed variation with strain rate and curvature is one of the objective of the project.

Lean combustion is receiving more concern while designing power generation units because of strict pollution norms. Lean combustion reduces the maximum flame temperature in combustor and reduces NOx formation, which is a measure contributor to pollution. In lean combustion, air-fuel mixture is close to lean flammability limit and improper mixing of air-fuel leads to spatial and temporal variation of mixture composition which can cause local mixture strength to go below lean flammability limit and may leads to local extinction. This local extinction results in the leakage of reactants which leads to reduction in heat release which in turn affects the overall efficiency of the device and leads to emission of pollutant as unburnt hydrocarbons.

Prediction of extinction based on mixture condition upstream of flame by applying the steady flammability limit(ϕ^*) criterion, that is if $\phi > \phi^*$, flame will sustain otherwise it will undergo an extinction, has found to be more restrictive and demands unnecessary high equivalence ratio for

CHAPTER 1. INTRODUCTION

stable combustion.

Counter-flow premixed flame configuration is widely used for the study of flame response to strain rate as axial velocity varies almost linearly from exit of the nozzle to central plane of symmetry. The strain rate at the flame decides the rate at which flow is diverging or converging while passing through the flame basing on the positive or negative sign. Flow divergence i.e positive strain rate increases heat loss from the flame and can lead to extinction if $Le > 1$ and vice versa.

One of the most fundamental issue in lean combustion is that whether flame will propagate or extinguish at specified local and temporal mixture condition [11]. So, by considering mixture condition upstream of the flame that is if local equivalence ratio(ϕ) is less than steady flammability limit(ϕ_s^*) for unstrained flat flame, one can expect local extinction. But it is observed that flame can sustain below ϕ_s^* . Since extinction is a combined effect of flow time scale, transport time scale and reaction time scales, dynamic flammability limit has been studied by Shankaran et.al. [11]. The proposed flammability limits are,

1. Steady Flammability Limit for unstrained flat flame(ϕ_s^*) : In general steady flammability limit is defined as minimum equivalence ratio above which steady flame can sustain without strain rate ($\kappa = 0$) and curvature.
2. Steady Flammability Limit (ϕ_s) : It is defined as minimum equivalence ratio above which steady flame can sustain, with strain rate may not equal to zero ($\kappa \neq 0$). Hence ϕ_s is a function of κ (i.e $\phi_s = f(\kappa)$)
3. Dynamic Flammability Limit(ϕ_t) : It is defined as minimum instantaneous equivalence ratio above which flame can sustain. So ϕ_t is the function of various parameters such as flow, transport and reaction time scales.

Bunsal et.al. [1] used dynamic flammability limit extension below steady flammability limit(ϕ_s) i.e. $(\phi_t - \phi_s)$ and normalized it with steady flammability margin, $(\bar{\phi} - \phi_s)$ and thus dynamic

CHAPTER 1. INTRODUCTION

flammability limit extension(*DFLE*) in normalized form is defined by,

$$DFLE = \frac{\phi_t - \phi_s}{\bar{\phi} - \phi_s} \quad (1.1)$$

Then *DFLE* is plotted against normalized equivalence ratio perturbation frequency for various strain rates. This normalized frequency(η) is selected so as to collapse unsteady extinction data on a single curve in *DFLE* – η plane which will separate inflammable region from nonflammable [see fig. 1.1]. This normalized frequency (η) is given by,

$$\eta = \delta \sqrt{\frac{\omega}{2D}} \quad (1.2)$$

where $\omega = 2\pi f$ is the angular frequency, and D is the mass diffusivity of major reacting species (CH_4) in reactant, and δ is the thermal flame thickness given by,

$$\delta = \frac{T_b - T_u}{(\nabla T)_{max}} \quad (1.3)$$

Here, δ is a function of both mean equivalence ratio and strain rate and hence incorporates both flame and flow time scales. Also δ^2/D is a measure of transport time scale through flame thickness.

The analysis by Bansal et al. [1] is basically for contour-flow configuration, hence to access the applicability of this extinction criterion for other configuration ‘slot stabilized flame’ configuration is selected. As $\phi = 0.6$ is close to lean flammability limit, it is selected as mean equivalence ratio for present work.

Ren Wu and Santosh [17], have investigated 2D slot stabilized premixed metane air flame with hot and cold co-flow. These cases are modelled with 4-step reduced mechanism. With cold co-flow local extinction is correctly predicted. As hot co-flow cases fall inside the inflammable region, no local extinction is observed on flame surface.

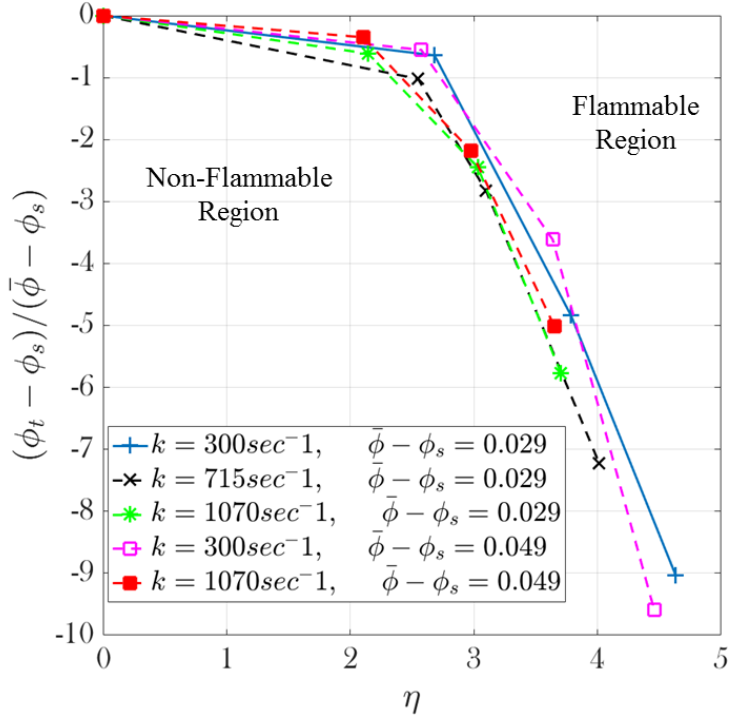


Figure 1.1: *DFLE* as a function of non-dimensional frequency (η)

Hence,in the present work local flame extinction phenomena on flame surface is investigated, with hot side walls adjacent to inlet exit and 15-step reaction mechanism with 19-species [13]. As this mechanism was derived from quasi steady state approximations (QSSA) for chemical species, validation of solver (MultiSolv) with this mechanism has been done by Kiran R. [10] with one dimensional flat flame by comparing laminar burning velocity, adiabatic flame temperature and flame-structure with detailed mechanism.

In present work, slot stabilized flame at mean equivalence ratio of 0.6, is studied for unperturbed and perturbed condition with perturbation amplitudes of, 5%, 20%, 40% of mean equivalence ratio. Before starting of perturbation cycles, flame is allowed to reach steady state at mean equivalence ratio ($\bar{\phi}$) and then analysis of flame is done to understand the physics behind the flame behaviour.

Equivalence ratio fluctuation causes heat release rate to oscillate either directly or indirectly. Fig 1.2 shows direct and indirect pathways. In case of direct influence, equivalence ratio

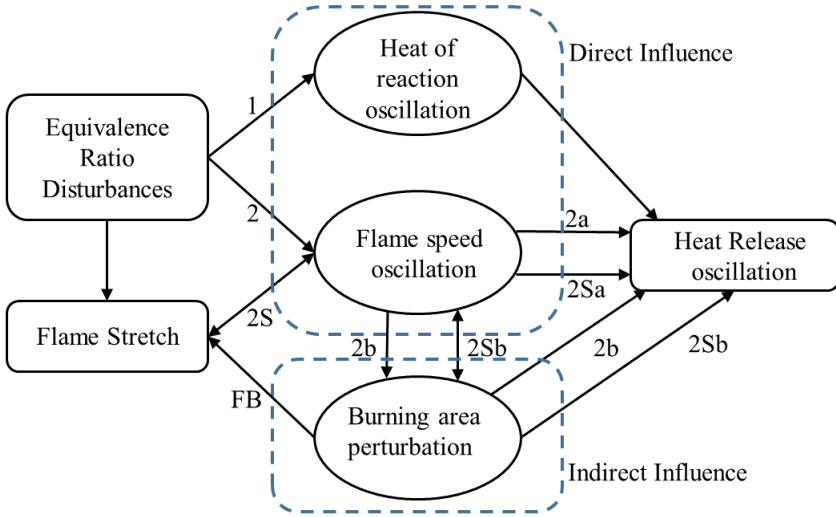


Figure 1.2: Equivalence ratio oscillation induced effects [12] (slightly modified)

fluctuation causes heat of reaction oscillation(path 1) and flame speed oscillation (path 2) which intern affect heat release rate directly and via (path 2a) respectively. Variation of equivalence ratio also leads to flame speed oscillations which affect the flame stretch(path 2S) and in turn stretch rate also affect the flame speed. This flame speed fluctuation affect heat release(2Sa). Flame speed oscillation causes burning area fluctuation(path 2b) which also affect flame speed(path 2Sb) and causes heat release oscillation via (path 2b,2Sb). Burning area perturbation gives feedback to flame stretch rate as flame stretch rate depends on flame shape(curvature) and surface velocity. If heat release oscillations are in unison with one or more acoustic modes of the system, can cause damage to the system.

Birbaud et al. [2] have studied non-linear response of inverted ‘V’ flame to equivalence ratio perturbation. They have noticed that at moderate amplitude of equivalence ratio wrinkle amplitude is sufficient enough to touch the outer boundary of reactant and detaches pocket of fresh reactant from the primary flame. This phenomena causes abrupt change in flame surface area and in turn net heat release rate.

1.1 Organization of Thesis

Solver description, grid generation, boundary conditions used for simulations are discussed in chapter 2. Analysis of steady state solution for unperturbed equivalence ratio is presented in chapter 3. Chapter 4, discusses about perturbed equivalence ratio cases, and results for steady flame with unperturbed equivalence ratio and perturbed equivalence ratio are also discussed.

Chapter 2

Formulation and Computational Setup

2.1 Solver Description

Present simulations are carried out using 'MultiSolv' solver. 'MultiSolv' is a DNS solver, developed at Combustion Physics Lab, Indian Institute of Science, Bangalore. It solves 3D compressible Navier-Stokes equations in generalized co-ordinates. For spatial derivatives explicit 8th order central difference scheme is used. An explicit 3rd order Runge-Kutta scheme is used for time marching. Solution is filtered at end of every 3rd time step with an explicit 10th order filter [6].

Species thermodynamic properties are calculated by NASA's thermodynamic data base. Transport properties of individual species are calculated by temperature fits from Gordon et al. [7]. Mixture averaged transport properties are used for simulations. Wilke's formulation is used to compute mixture average viscosity [16] and Warnatz's formulation is used to compute mixture averaged thermal conductivity [5]. Species diffusivities are computed by using a constant Lewis number assumption for each species as it's variation is small in flame front [9]. Lewis number for individual species is obtained from Chen et al. [4].

Characteristic boundary conditions are used for Navier-Stokes equations, at boundaries

CHAPTER 2. FORMULATION AND COMPUTATIONAL SETUP

by assuming locally one dimensional(LODI) flow [8].

Solver uses Message Passing Interface (MPI) to perform parallel computing. Solver uses multi-block structured grid as input, and assign each processor to individual block [14]. For every iteration neighbouring blocks exchanges data to maintain solution and domain continuity. Explicit scheme reduces communication time by reducing amount of data transfer required.

2.2 Case Setup

2.2.1 Grid Generation

Multiblock Structured grid is used for present simulations. Fig 2.1 shows schematic of slot stabilized flame for present study and fig 2.2 shows actual grid with each and every point. Simulations with $\epsilon = 0.05, 0.2$, are using same grid with minimum grid spacing of $40\mu m$. This minimum grid spacing is maintained along axial x-direction downstream of inlet exit, up to $7R$ length. After that grid is stretched up to outlet. As x-axis is an axis of symmetry, grid spacing along positive and negative y-axis is maintained $40\mu m$ in region of $3R$ from x-axis. After that grid is stretched up to side wise outlets.

For this simulation 2.4million points are used with 965 blocks. Hence every block has around 2500 points. For $\epsilon = 0.4$ case, minimum grid spacing of $35\mu m$ is used by maintaining all other configurations same.

2.2.2 Initial Condition and Boundary Conditions

In this project slot stabilized 2D flame configuration for CH_4 Air mixture is studied for mean equivalence ration of 0.6 ($\bar{\phi} = 0.6$). Inlet velocity is maintained constant for all simulations, and magnitude is fixed to get flame height six times the inlet radius ($L_f = 6R$). For that, Laminar

CHAPTER 2. FORMULATION AND COMPUTATIONAL SETUP

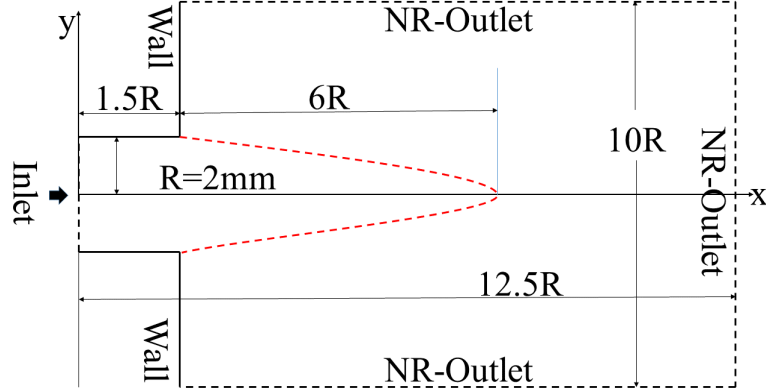


Figure 2.1: Schematic of 2D slot stabilized flame used for present simulations

flame speed (S_L) at $\bar{\phi} = 0.6$ is computed from CANTERA [3] and then,

$$u = S_L / \sin(\theta)$$

gives inlet velocity(θ is half cone angle of flame). Initial conditions are setup by assuming conical shape of flame so as to reach the steady state solution quickly. By using CANTERA [3] adiabatic flame temperature (T_{ad}) and equilibrium mass fractions of species($Y_{i,eq}$) are computed using initial reactant state as temperature 300K, pressure 1atm and equivalence ratio of 0.6. Temperature and species mass fraction profiles are initialized with hyperbolic tangent function to have smooth variation from unburnt to burnt state across assumed conical flame shape[see fig. 2.3].

To anchor flame at inlet exit, same temperature profile as inside the domain for initial condition is applied on the walls. No-slip wall condition is used for the walls and species's flux normal to the walls are set to zero by imposing,

$$(\nabla Y_i) \cdot \hat{n}_w = 0 \quad (2.1)$$

, at the wall.

At inlet 'characteristic non-reflecting inlet' boundary condition is applied. At axial outlet and for two sideways outlets 'characteristic non-reflecting outlet' boundary condition is applied

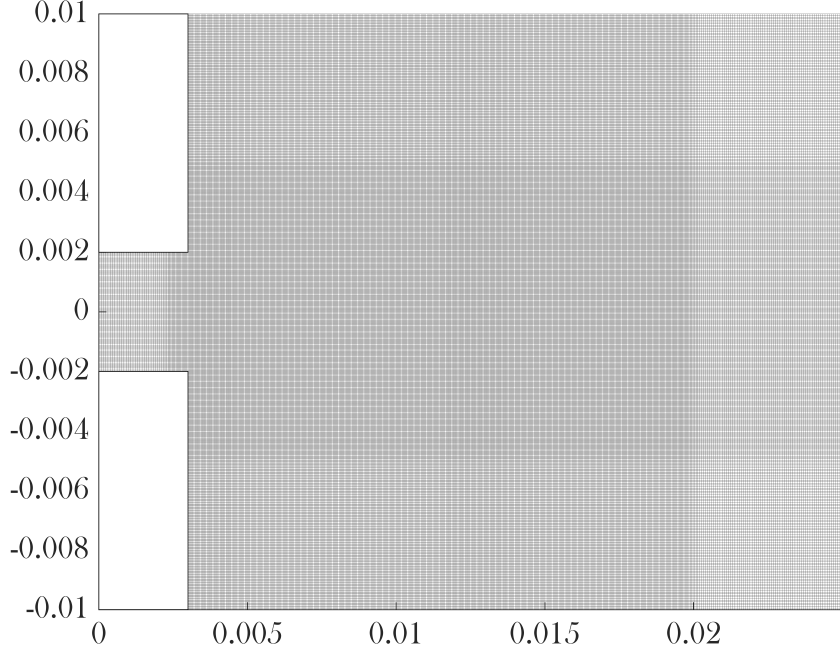


Figure 2.2: Mesh used for present simulations with every point in the grid (fine mesh in the flame region and stretched outside)

[8]. Periodic boundary condition is applied on domain boundaries normal to z-axis. $CFL = 0.5$ is used for all simulations.

2.2.3 Forced Case

After obtaining the steady state, the solution is used as initial condition for simulating perturbed cases with normalized Y_{CH_4} perturbation amplitude $\epsilon = 0.05, 0.2, 0.4$. Hence, equivalence ratio at inlet as a function of time is given by,

$$Y_{CH_4} = Y_{CH_4,0}[1 + \epsilon \sin(2\pi f t)] \quad (2.2)$$

Here, $Y_{CH_4,0}$ is the CH_4 mass fraction corresponding to mean equivalence ratio. Using Strouhal number, $St = L_f f / u = 1$, excitation frequency comes out to be $f = 60Hz$. While, perturbing equivalence ratio at inlet, density is maintained constant to specifically study equiva-

CHAPTER 2. FORMULATION AND COMPUTATIONAL SETUP

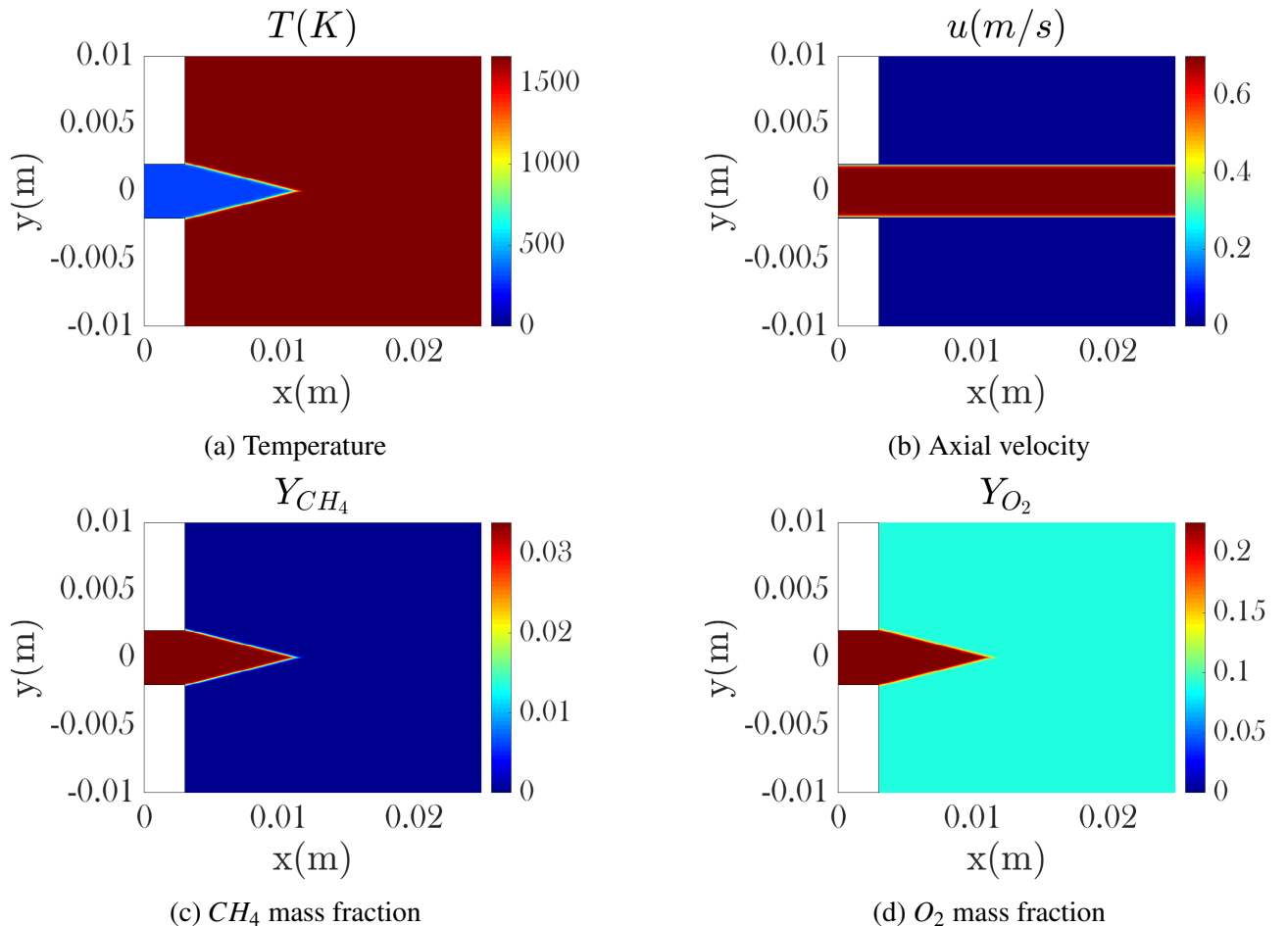


Figure 2.3: Initial conditions for Temperature and species which vary from un-burnt to burnt state across the flame.(b) Axial velocity initialized with same profile as at inlet.

CHAPTER 2. FORMULATION AND COMPUTATIONAL SETUP

lence perturbation effect on flame response. Constant Density is achieved by maintaining constant molecular weight of mixture (MW_{mix}) by adjusting Y_{O_2}, Y_{N_2} according to Y_{CH_4} ,

$$Y_{O_2}(t) = k_1 - k_2 Y_{CH_4}(t) \quad (2.3)$$

$$Y_{N_2}(t) = 1 - Y_{CH_4}(t) - Y_{O_2}(t) \quad (2.4)$$

Where k_1 and k_2 are,

$$k_1 = \frac{1 - (MW_{N_2}/MW_{mix})}{1 - (MW_{N_2}/MW_{O_2})} \quad (2.5)$$

$$k_2 = \frac{1 - (MW_{N_2}/MW_{CH_4})}{1 - (MW_{N_2}/MW_{O_2})} \quad (2.6)$$

This equivalence ratio oscillations affects heat release rate directly and indirectly, and also gives rise to flame surface oscillations as discussed in chapter 1.

Chapter 3

Steady State

Steady state results of simulation with $\phi = 0.6$ are used for investigating the effect of strain rate(κ), curvature(C) on flame speed(S_L). Fig 3.1 shows steady state temperature field with heat release rate contours in black color and vector velocity field (\vec{V}). It can be noticed that flow diverges while passing through the flame.

Some species fields are shown in fig 3.2 where black colour contour shows heat release zone. CO has higher concentration in heat release zone, while H and OH shows higher concentration around flame but in high temperature region next to heat release zone and H_2 shows higher concentration around flame but on reactant side before heat release zone.

3.1 Flame Speed Calculation

Laminar flame speed $S_{L,0}$ of unstrained flat flame is a fundamental quantity and it's accurate measurement has vital importance in combustion. In order to validate solver for 2D-combustion simulations, flame speed (S_L) is computed based on unburnt reactants flow velocity and compared with standard flame speed. For that, $T = 350K$ contour is selected [see fig. 3.3].

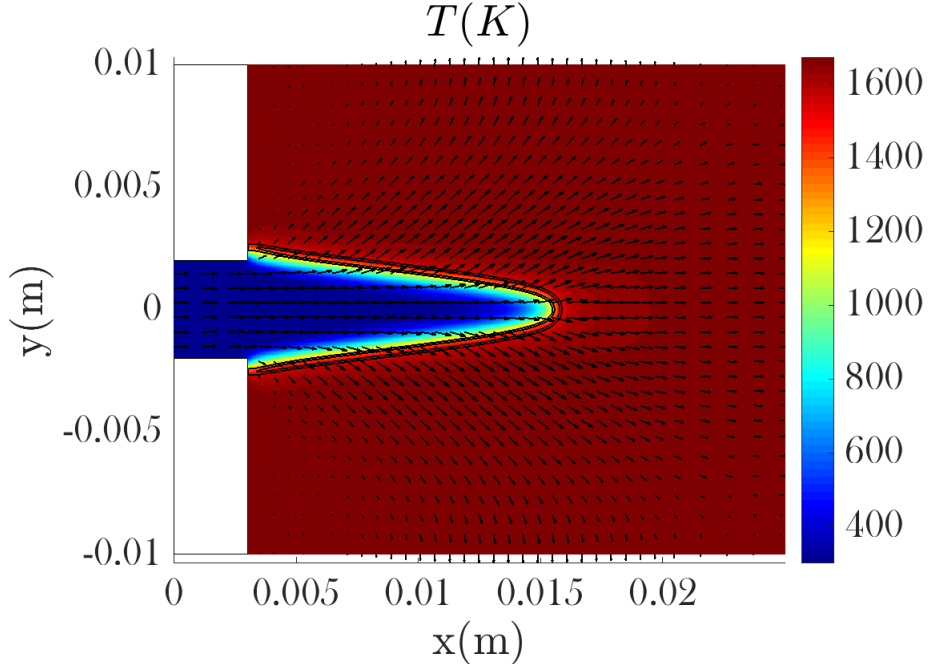


Figure 3.1: Temperature field with Heat Release rate contour in black and overlapped velocity vector field

Then flame speed $S_{L,u}$ is computed by,

$$S_{L,u} = -\vec{V} \cdot \hat{n} \quad (3.1)$$

,here \hat{n} is unit vector normal to contour and points into the reactants where \vec{V} is flow velocity.

As contour is single valued in terms of y , spline fit is used for contour data to get $x = f(y)$. Then unit normal to contour at (x, y) is calculated by,

$$\hat{n} = \frac{-\hat{e}_x + f_y \hat{e}_y}{\sqrt{1 + f_y^2}} \quad (3.2)$$

Flame speed (S_L) variation from flame base to tip along the x-axis is shown in fig. 3.4. At starting flame speed is zero ($S_L = 0$), that is because of zero flow velocity at wall. Flame

CHAPTER 3. STEADY STATE

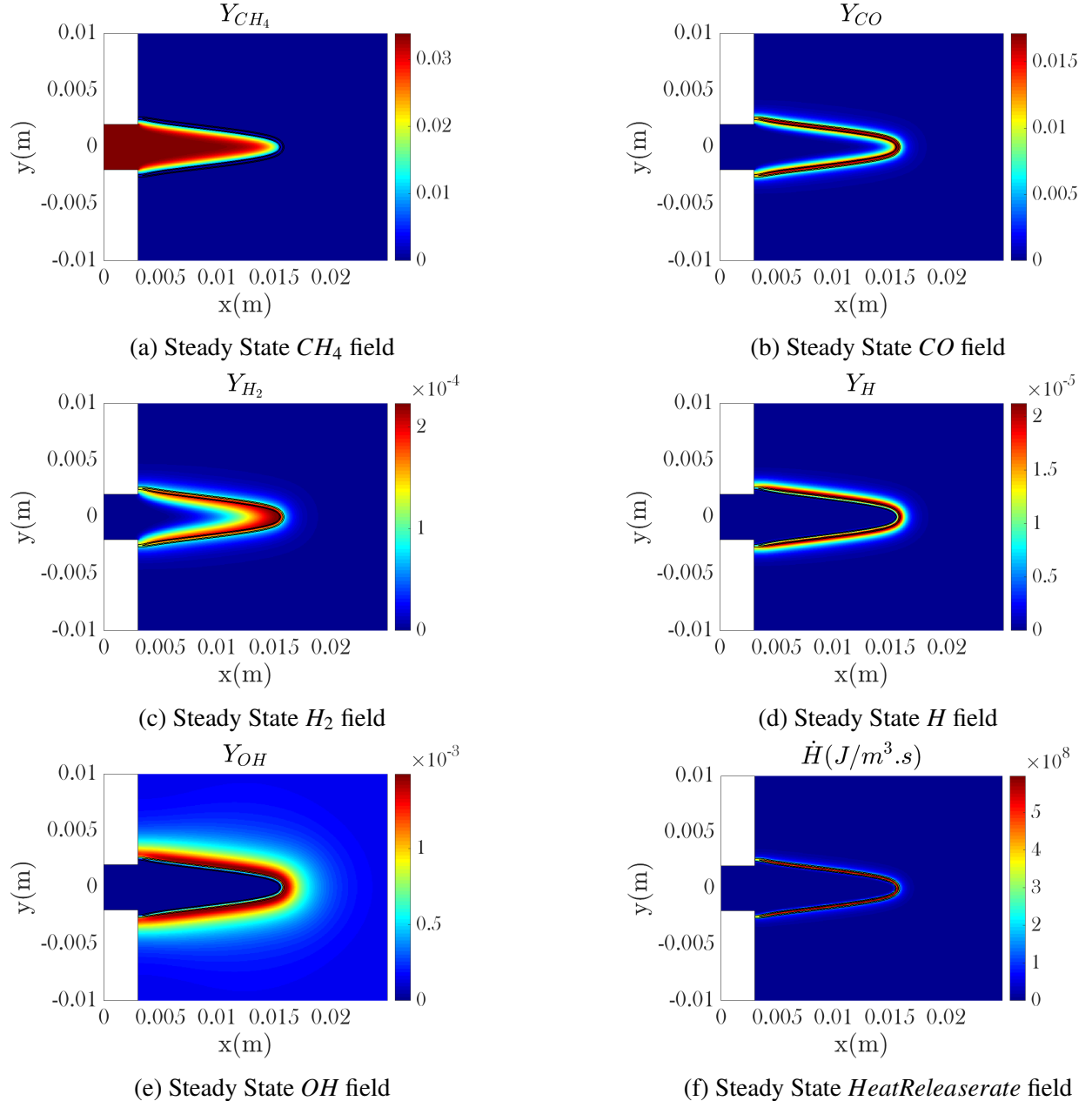


Figure 3.2: Steady State fields for CH_4 , CO , H_2 , H , H_2 and Heat Release rate per unit volume (\dot{H})

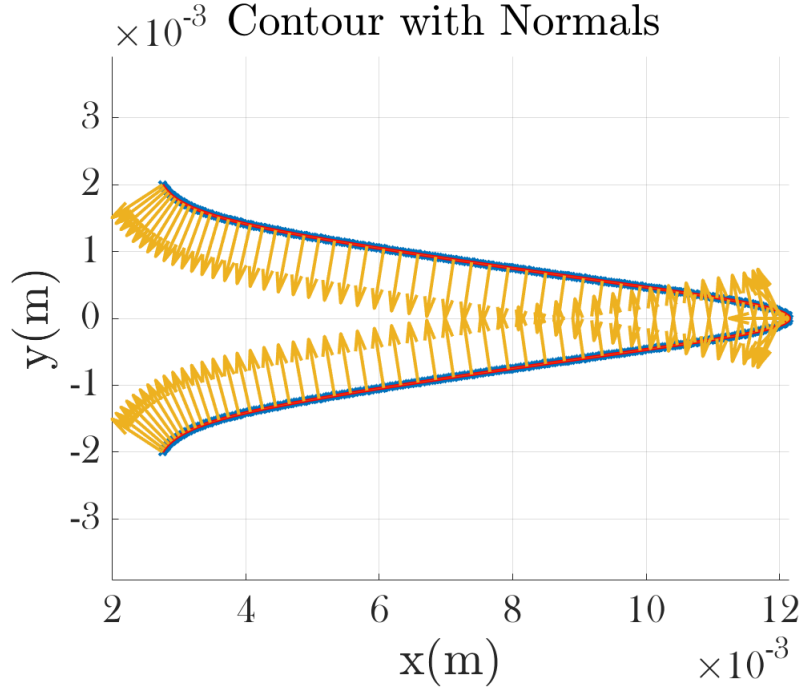


Figure 3.3: Normal to the contour of T=350K

speed, then increases because of reduced wall effect and becomes almost constant as flame surface is almost flat in this region. Finally at flame tip, S_L attains its maximum value which is close to 0.8 m/s.

3.2 Curvature effect on flame speed

Fig 3.5 shows curvature variation from flame base to flame tip. Curvature (C) is calculated by,

$$C = \frac{f_{yy}}{(1 + f_y^2)^{3/2}}$$

. Fig 3.5 shows, curvature is negative and has high magnitude at flame tip. Therefore S_L rise at flame tip is mainly because of curvature. Fig 3.6 shows variation of S_L with curvature (C).

From fig 3.6, most of the the points are clustered about zero curvature and S_L behaviour is non linear close to zero curvature. To calculate flame speed for flat flame, local minima from high flame speed branch which close to $C = 0$ is measured an it is $S_{L,min}=0.134(m/s)$. As contour

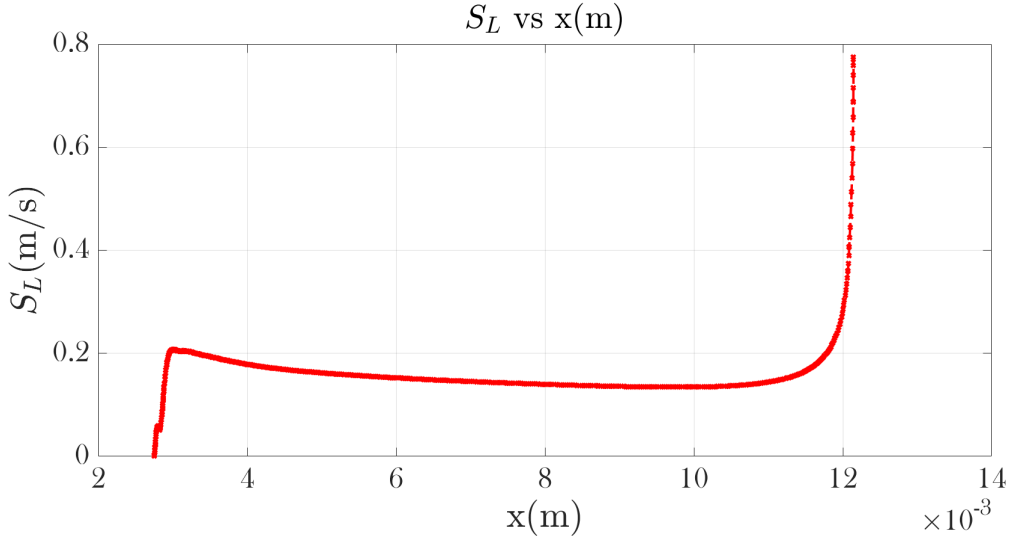


Figure 3.4: Axial variation of $S_L(m/s)$

is at $350K$, S_L for $300K$ comes out to be $0.115(m/s)$ and from CANTERA [3] with detailed mechanism S_L is $0.1155m/s$ which is a quite close match.

3.3 Strain rate (κ) effect on Flame Speed

For strain rate calculation, contour of $T = 350K$ is selected same as that of curvature calculation. Then tangential strain rate [9] is calculated by,

$$\kappa = (\delta_{ij} - n_i n_j) \frac{\partial u_i}{\partial x_j} \quad (3.3)$$

where, δ_{ij} is kronecker delta, n_i is i^{th} component of unit normal to flame surface (\hat{n}) and u_i is i^{th} component of flow velocity.

Fig 3.8 shows S_L variation with strain rate (κ). Near flame base, because of wall effect, curve does not have proper behavior. For intermediate region where strain rate is higher as compared to curvature, flame speed increases with strain rate. For higher strain rate curve is almost linear but near zero strain rate S_L behaves non-linearly with strain rate. For flame surface near tip where strain rate is small but flame speed reaches peak value because of high curvature. To

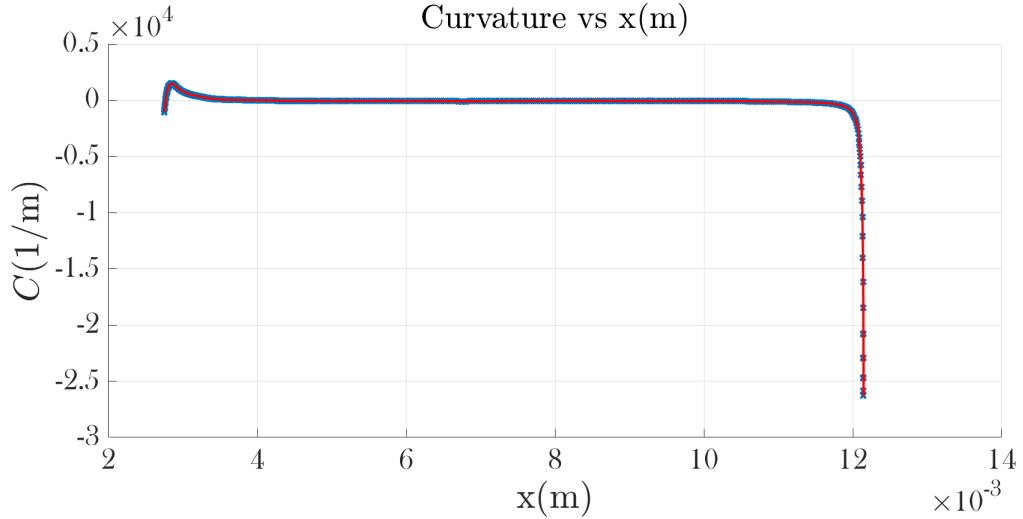


Figure 3.5: Axial variation of curvature ($C(1/m)$)

calculate flame speed for un-strained flame, at zero strain rate point flame speed is measured as $S_L = 0.139(m/s)$, as it is measured at $350K$ for $300K$, S_L is $0.1191(m/s)$ and standard value is $0.1154(m/s)$. This deviation is because of non-zero curvature at selected point.

Fig 3.8, shows the plot for intermediate flame surface which corresponds to small flame curvature, and flame speed behaves linearly with strain rate. Sensitivity of flame speed(S_L) to strain rate (κ), is defined as Markstain length. Fig 3.9 shows that slope is $0.000505m$ which is the flame speed sensitivity to strain rate and negative of slope is Markstain length, $L_u = -0.505mm$ and $S_{L,\kappa=0}$ is $0.14287m/s$ which is for $T = 350K$, means $0.12246(m/s)$ for $300K$. Fig. 3.10 shows comparison of computed Markstain length(L_u) with Varea et al. [15] measurement.

CHAPTER 3. STEADY STATE

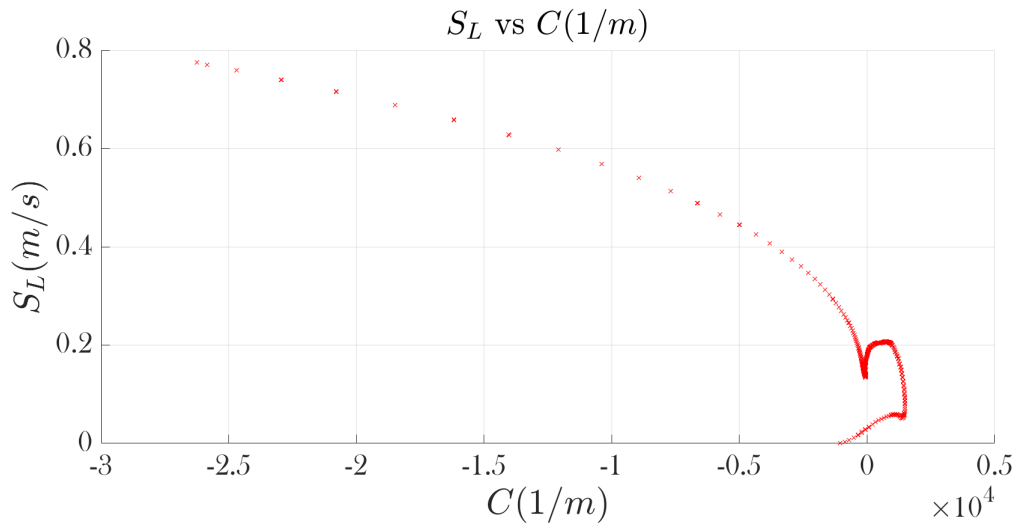


Figure 3.6: Variation of flame speed (S_L) with curvature ($C(1/m)$)

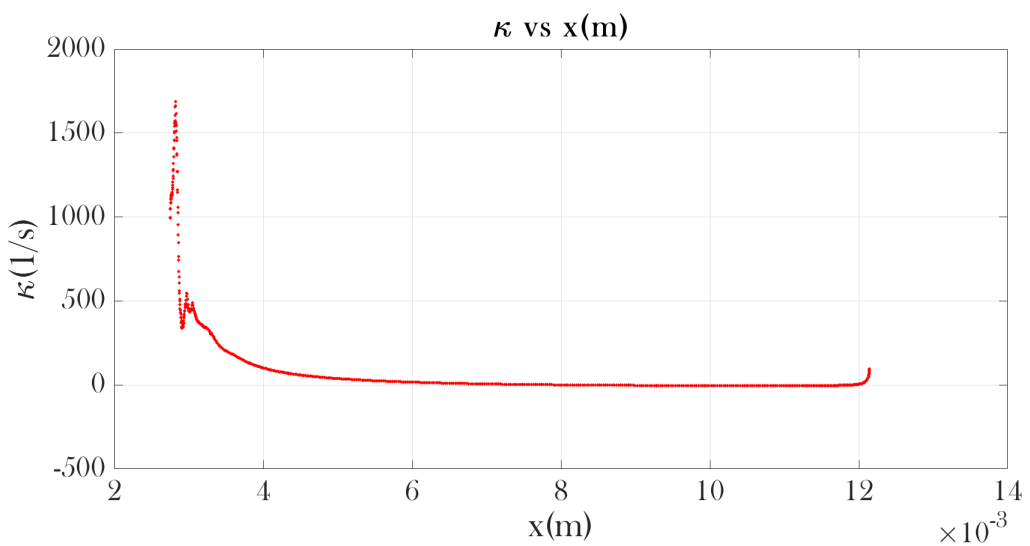
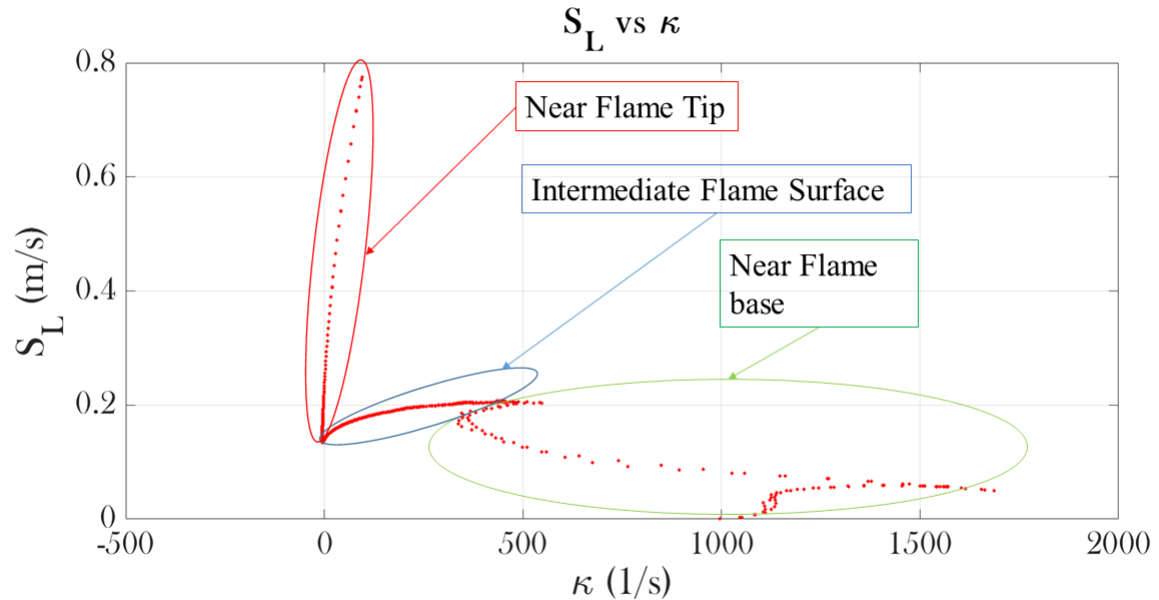
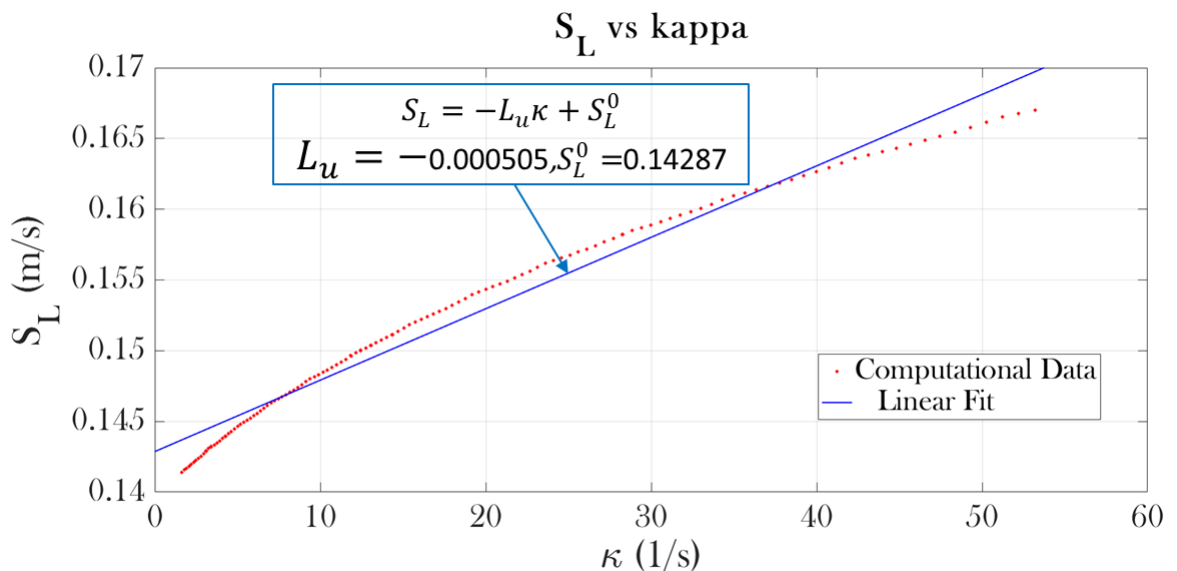


Figure 3.7: Axial variation of Strain Rate ($\kappa(1/s)$)


 Figure 3.8: Variation of flame speed (S_L) with Strain Rate ($\kappa(1/s)$)

 Figure 3.9: Flame speed(S_L) vs strain rate(κ) with linear fit.

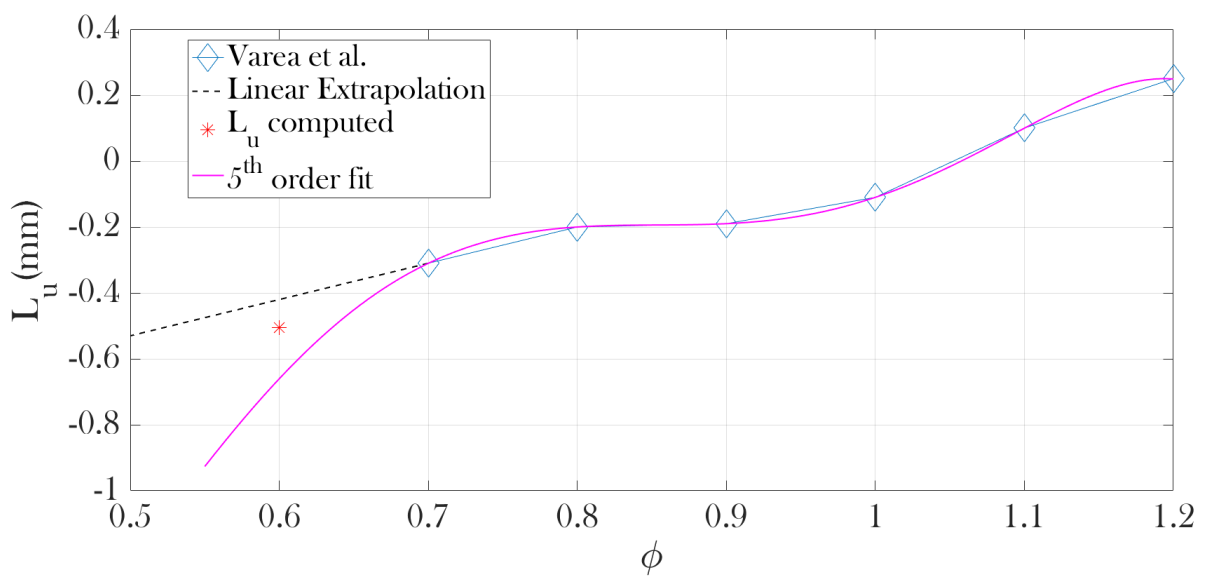


Figure 3.10: Comparison of Markstain length by Varea et al. [15] with computed L_u

Chapter 4

Perturbed Cases

Simulations are performed for mean equivalence ratio of $\bar{\phi} = 0.6$ and normalized perturbation amplitude $\epsilon = 0.05, 0.2, 0.4$. As discussed in chapter 1, normalized minimum equivalence ratio and normalized forcing frequency decides the behaviour of flame that whether it will sustain or extinguish. Fig 1.1 shows inflammable and non-flammable regions separated by $DFLE(\eta)$ curve.

For all simulations maximum extension of equivalence ratio below steady flammability limit ($\phi_{min} - \phi_s$), is normalized with flammability margin, and can be given by,

$$\phi_{min}^* = \frac{\phi_{min} - \phi_s}{\bar{\phi} - \phi_s} \quad (4.1)$$

Table 4.1 shows ϕ_{min}^* calculations,

ϵ	$\bar{\phi}$	ϕ_{min}	ϕ_s	ϕ_{min}^*
0.05	0.6	0.57	0.56	0.25
0.2	0.6	0.48	0.56	-2.0
0.4	0.6	0.36	0.56	-5.0

Table 4.1: Normalized minimum equivalence ratio(ϕ_{min}^*) Calculation

CHAPTER 4. PERTURBED CASES

Equivalence ratio perturbation frequency is normalized by,

$$\eta = \delta \sqrt{\frac{\omega}{2D}}, \quad (4.2)$$

where, $\omega = 2\pi f$ is the angular frequency, D is the mass diffusivity of major reacting species (CH_4) in reactant, and δ is the thermal flame thickness given by,

$$\delta = \frac{T_b - T_u}{(\nabla T)_{max}} \quad (4.3)$$

, where T_b and T_u are burnt and unburnt gas temperature respectively($T_b = 1665K$ and $T_u = 300K$). δ is measured at $3R$ from flame base and is $0.915mm$. Diffusivity of CH_4 at $300K$ is $2.3031 \times 10^{-5} m^2/s$. Hence,

$$\eta = 2.6177 \quad (4.4)$$

Each case is plotted on fig. 1.1 for respective ϕ_{min}^* and η values. Fig 4.1 shows this plot,

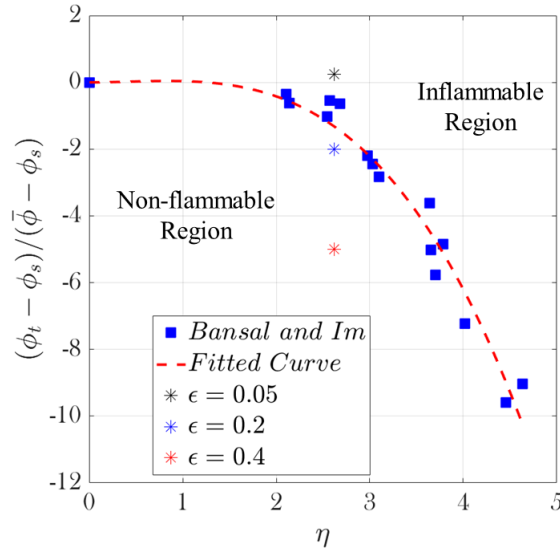


Figure 4.1: Plot of present cases on figure 1.1

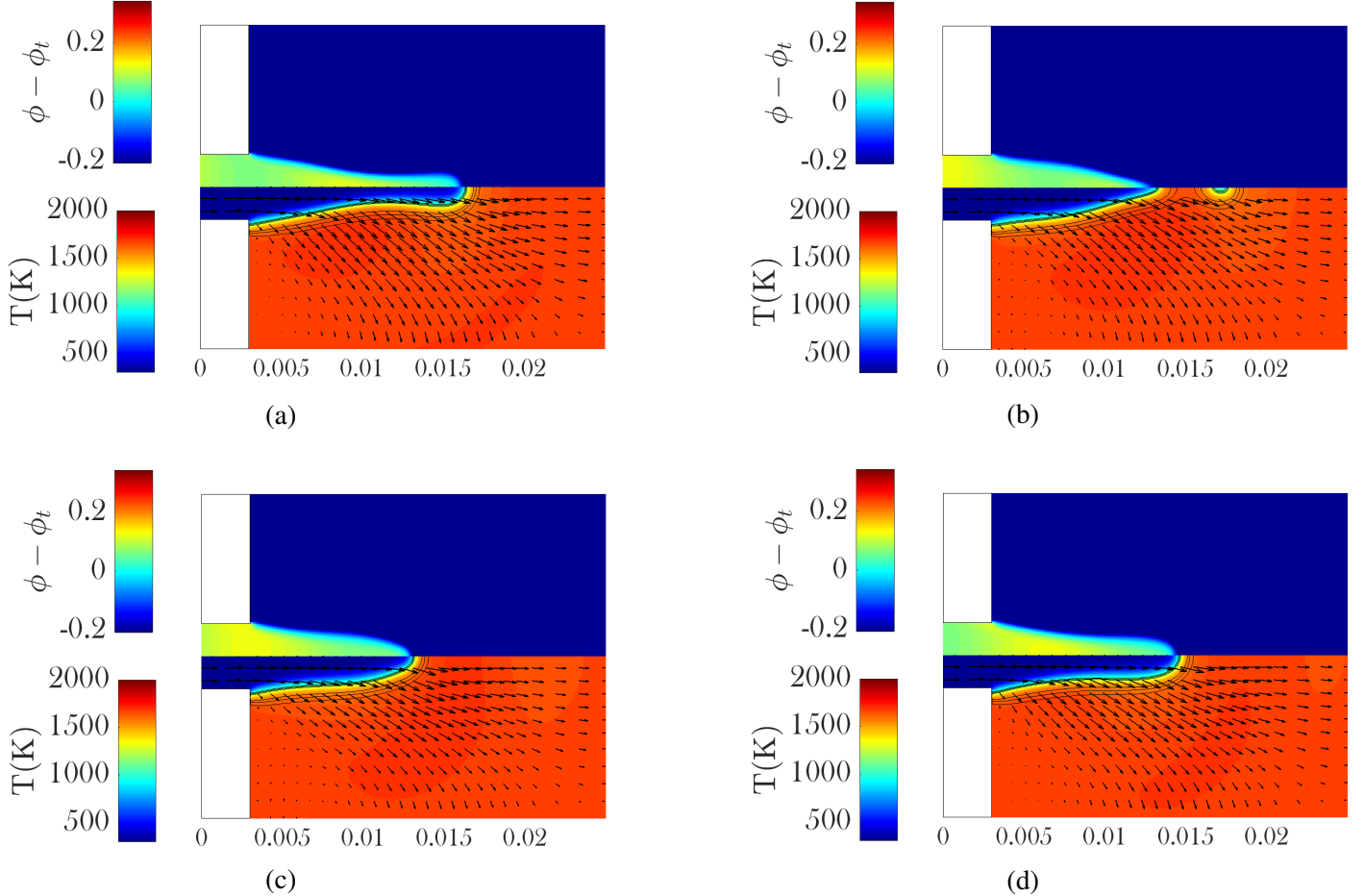


Figure 4.2: Comparative plots of $(\phi - \phi_t)$, Temperature(K) fields with Hear release rate(\dot{H}) contours and velocity vector field for different phase angles at Inlet ($\bar{\phi} = 0.6$, $\epsilon = 0.05$, $f = 60Hz$)

In fig. 4.1 black colour curve is obtained by fitting cubic polynomial to $DFLE - \eta$ data (blue boxes) from fig 1.1. Figure 4.1 shows that $\epsilon = 0.05$ case lies in inflammable region, where as $\epsilon = 0.2$ and 0.4 , lies in non-flammable region.

4.1 Case: $\epsilon = 0.05$

Fig. 4.2 shows $\phi - \phi_t$ field and temperature(T) field at various phases of perturbation cycle at inlet. Here ϕ_t is the dynamic flammability limit for corresponding normalized frequency(η). Contours of heat release rate are shown in black. Levels for this contour are at 5%, 10%, 20% of

CHAPTER 4. PERTURBED CASES

maximum heat release rate for steady unperturbed case.

In figure 4.2a flame is contracted and has narrow shape near tip. This is because of mixture with higher equivalence ($\phi > \bar{\phi}$) ratio is passing through this region. This mixture causes increase in flame speed, than the flame speed at mean equivalence ratio($\bar{\phi}$) which causes imbalance in flame normal flow velocity and flame speed, hence flame propagate into the reactants and changes the flame shape.

In fig. 4.2b there is detached pocket from the original flame. In fig. 4.2a, there is lower equivalence ratio mixture($\phi < \bar{\phi}$) is at flame tip and upstream of that there is mixture with higher equivalence ratio ($\phi > \bar{\phi}$). So, $\phi > \bar{\phi}$ mixture burns quickly than $\phi < \bar{\phi}$ mixture which is at tip and causes detachment of mixture pocket with $\phi < \bar{\phi}$.

In fig. 4.2c there is no detached pocket as it is burned out because of hot surrounding. In fig. 4.2d there is lower equivalence ratio mixture is at flame tip($\phi < \bar{\phi}$) and upstream of that there is mixture with higher equivalence ratio ($\phi > \bar{\phi}$) which gives rise to flame shape as fig. 4.2a.

As heat heat release rate contours are continuous, there is no local extinction of flame as expected from fig 4.1.

4.2 Case: $\epsilon = 0.2, \epsilon = 0.4$

Fig 4.3, 4.4 shows $\epsilon = 0.2$ and 0.4 cases respectively with $(\phi - \phi_t)$ field and temperature(T) field at various phases of perturbation cycle at inlet and contours of heat release rate are shown in black at 5%, 10%, 20% of maximum heat release rate for steady unperturbed case. Similar to $\epsilon = 0.05$ case, pocket of lower mixture strength is formed which eventually get consumed because of hot surrounding.

Fig 4.3a and 4.4a shows the 0° phase at inlet. It is observed that flow inside the domain is directed away from the flame. Heat release on flame surface is causing an expansion of fluid while passing through it and forcing the flow away from the flame.

CHAPTER 4. PERTURBED CASES

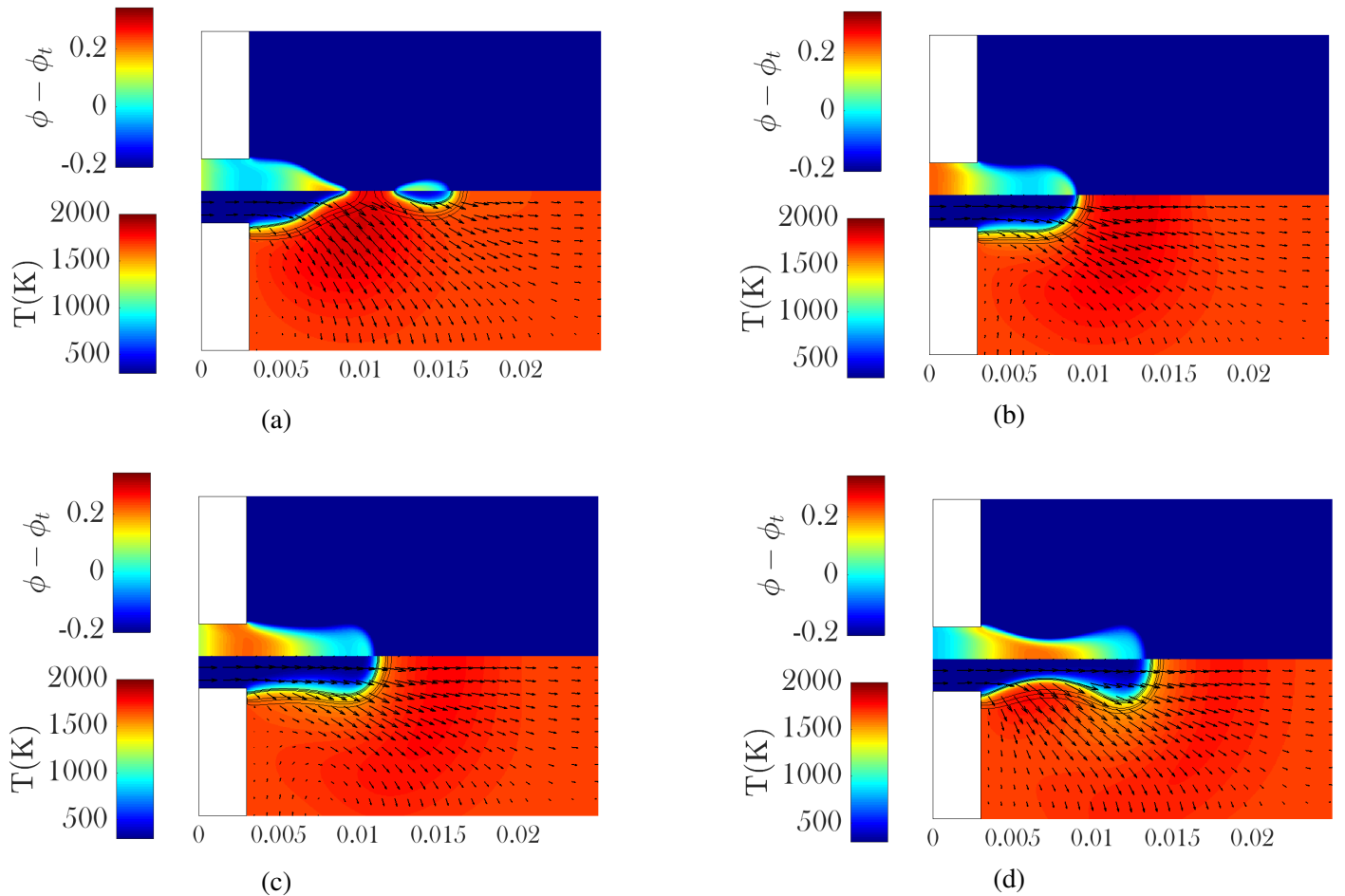


Figure 4.3: Comparative plots of of $(\phi - \phi_t)$, Temperature(K), Hear Release Rate contours and velocity vector field for different phase angles at Inlet ($\bar{\phi} = 0.6$, $\epsilon = 0.2$, $f = 60Hz$)

CHAPTER 4. PERTURBED CASES

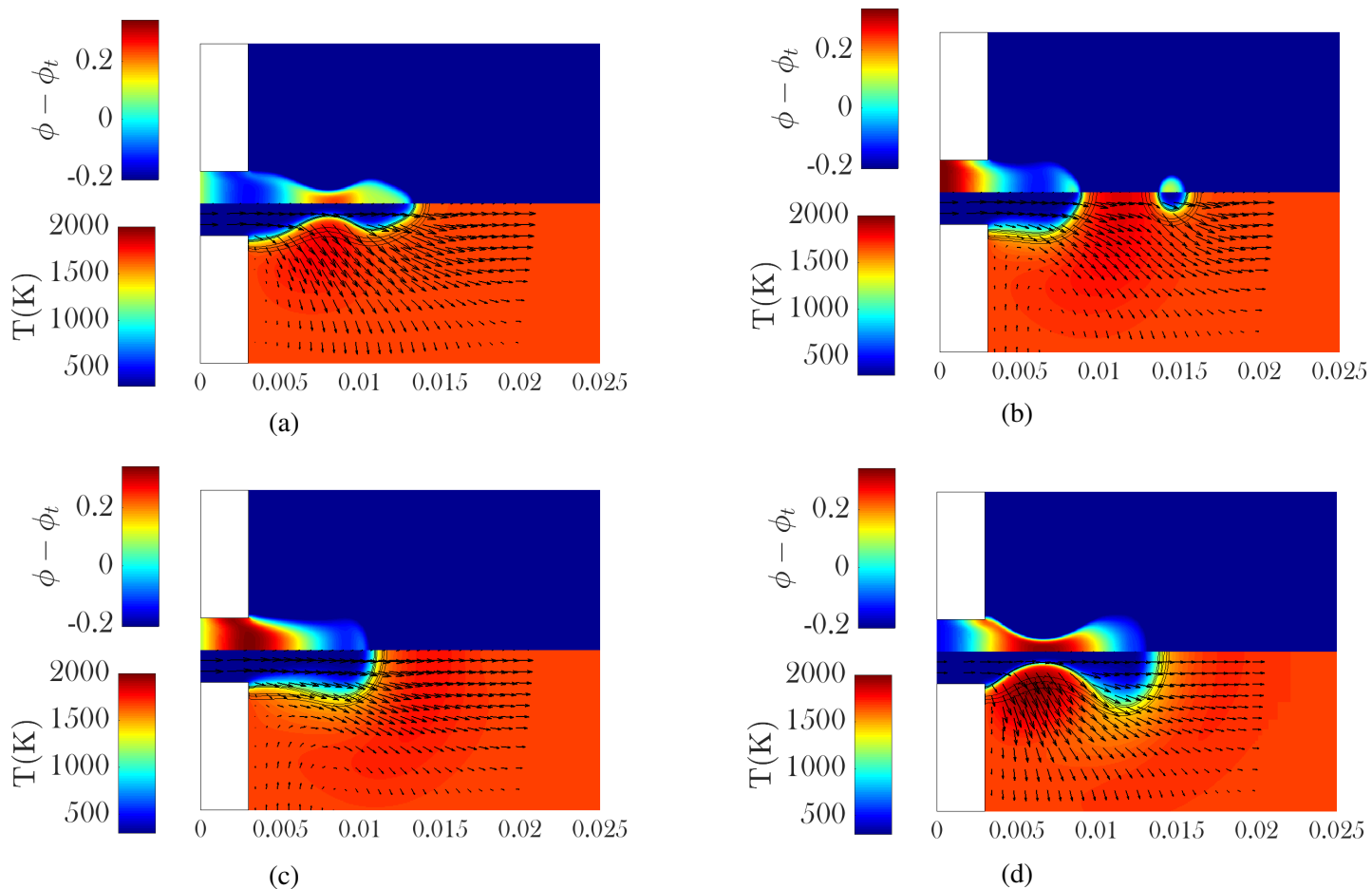


Figure 4.4: Comparative plots of of $(\phi - \phi_t)$, Temperature(K), Hear Release Rate contours and velocity vector field for different phase angles at Inlet ($\bar{\phi} = 0.6$, $\epsilon = 0.4$, $f = 60Hz$)

CHAPTER 4. PERTURBED CASES

Fig. 4.3b and 4.4b, show that the flow pattern around the flame is modified. Near wall hot flow of products is directed towards the flame. This can be explained by fig. 4.5. Low equivalence ratio mixture produces less dilatation rate than higher equivalence ratio mixture, hence as low equivalence ratio mixture approaches to flame dilation rate at flame reduces and causing reduction in pressure near wall [see fig 4.5a]. This pressure gradient causes flow of hot gas towards the flame. This hot flow towards the flame base is supporting the combustion of mixture with lower equivalence ratio. In fig 4.5b, pressure surrounding the flame is below atmospheric pressure. Region between primary flame and detached packet have additional pressure drop this is because of heat transfer from this region to primary flame and lean pocket, causing reduction in temperature and hence drop in pressure.

Fig. 4.5c shows that, as higher equivalence ratio mixture approaches to flame pressure around flame has raised above atmospheric pressure and position of vortex has slightly pushed away from the flame. In fig 4.5d, because of intense combustion of higher equivalence ratio mixture, pressure inside flame is substantially increased because of high dilatation rate, this forces the flow from flame to outlets.

4.2.1 Extinction Analysis:

Fig. 4.6 shows, heat release rate contours for 5%, 10% and 20% of maximum heat release rate($\dot{H}_{max,ss}$) at steady state. Contour for $0.2\dot{H}_{max,ss}$, is broken near tip. Means \dot{H} has reduced less than $0.2\dot{H}_{max,ss}$ inside the flame that lies within yellow circle. But still contours of $0.05\dot{H}_{max,ss}$ and $0.1\dot{H}_{max,ss}$ are continuous, shows that reactions are not quenched. The reason for this non-quenching of reactions is mostly because of curvature effect.

Species OH , HO_2 are main contributors to branching and termination reactions respectively. Sankaran et. al [11] have suggested a parameter β which compares branching reaction rate with termination reaction rate,

$$\beta = \frac{w_b/w_t}{(w_b/w_t)_{\bar{\phi}}}. \quad (4.5)$$

CHAPTER 4. PERTURBED CASES

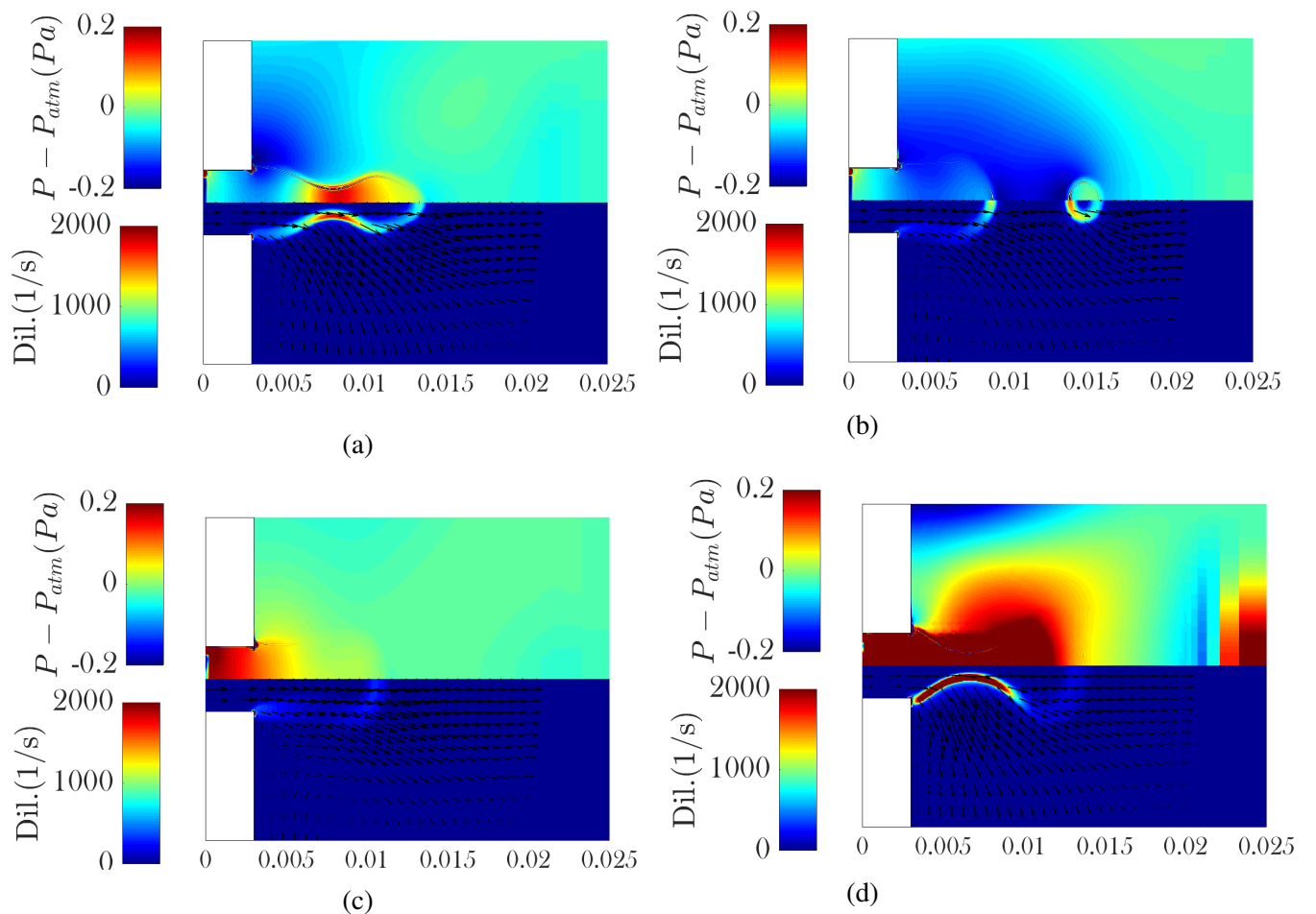


Figure 4.5: Comparative plots of of $(P - P_{atm})$ and Dilatation rate(1/s) field($\bar{\phi} = 0.6$, $\epsilon = 0.4$, $f = 60Hz$)

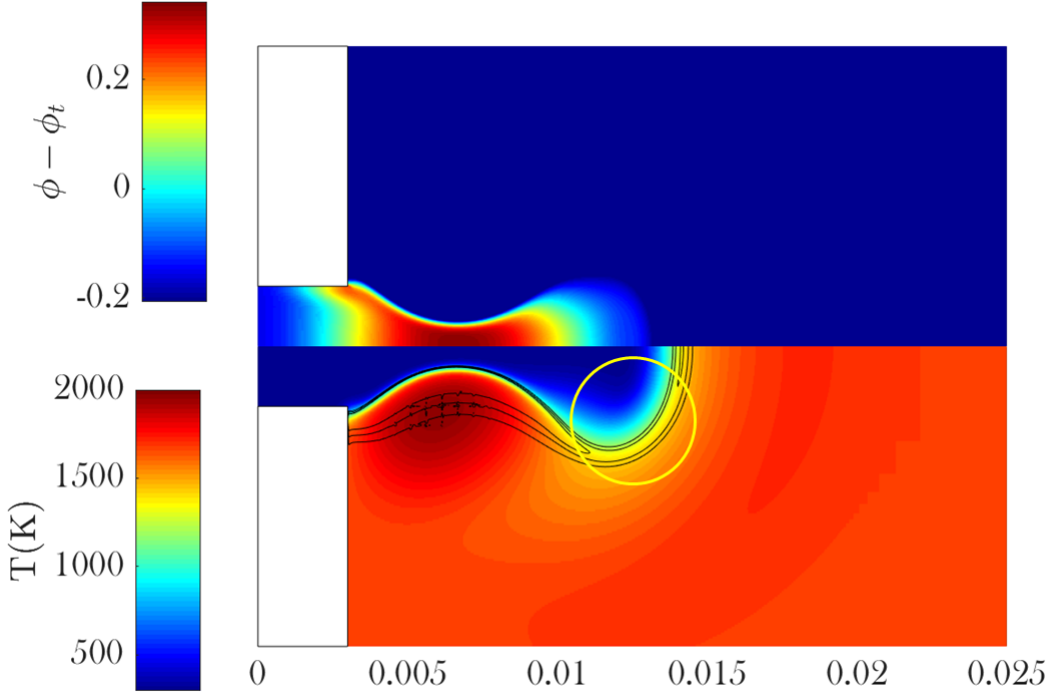


Figure 4.6: Comparative plot of $\phi - \phi_t$ and Temperature(K) field with heat release rate contour(\dot{H}) for $\bar{\phi} = 0.6$, $\epsilon = 0.4$, $f = 60\text{Hz}$ case.

β is the ratio of reaction rate of branching and termination reactions and normalized with respect to steady state maximum value of ratio of reaction rate of branching and termination reactions. Parameter β is measured at maximum w_b location. Since w_b is branching reaction rate, w_{OH} is used to get approximate rate of branching reaction and w_{HO_2} is used as to get rate of termination reaction.

Fig 4.7 shows plot of parameter β measured at maximum w_b location along y-direction for given axial co-ordinate. Dotted red line shows flame tip, based on maximum heat rate. Sankaran et.al [11] have noticed that on quenching of reactions β suddenly drops to zero. The plot 4.7 shows that β takes value close to unity over the flame implies that there is no quenching of reactions. The sudden drop after peak is because of crossing the flame height and not because of quenching of reactions.

Fig 4.8, shows \dot{w}_{CH_4} for steady state and for $\epsilon = 0.4$ case at 270° phase angle at inlet. Molar consumption rate of CH_4 is nothing but rate of chain initiation reaction. Fig 4.9 shows

CHAPTER 4. PERTURBED CASES

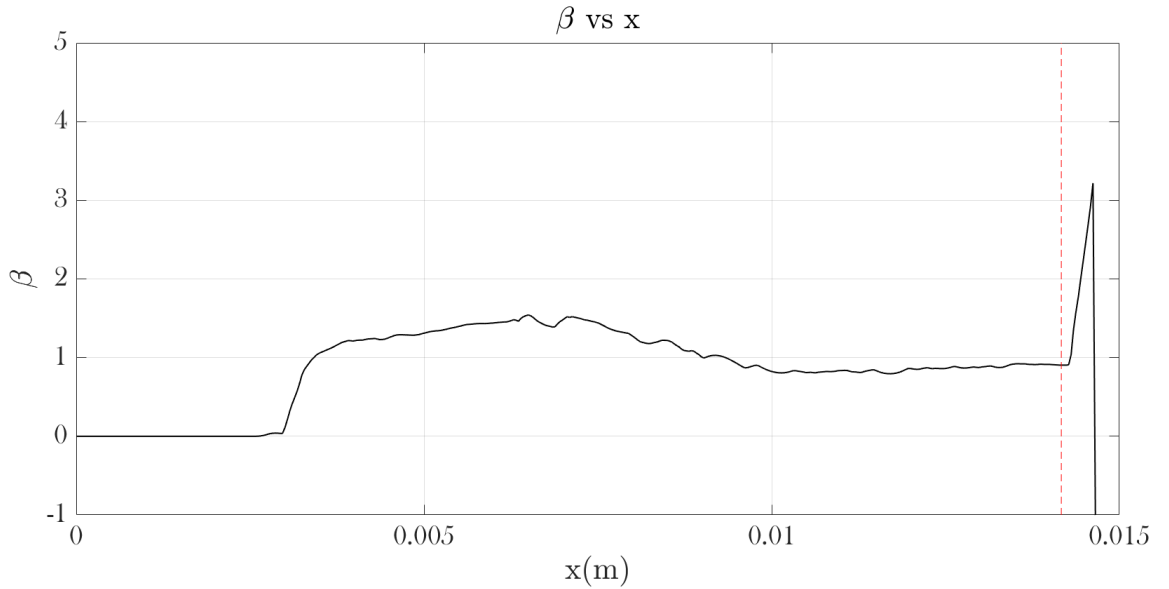


Figure 4.7: Plot of parameter β along axial direction.

volumetric molar production(destruction) rate of H , H_2 , OH which is directly related to branching reaction rate. Fig 4.10 shows volumetric molar production(destruction) rate of HO_2 which is related to termination reaction. It can be seen that near flame tip branching as well as termination reactions have reduced reaction rate, but still from 4.7 plot, their ratio is comparable to steady state.

CHAPTER 4. PERTURBED CASES

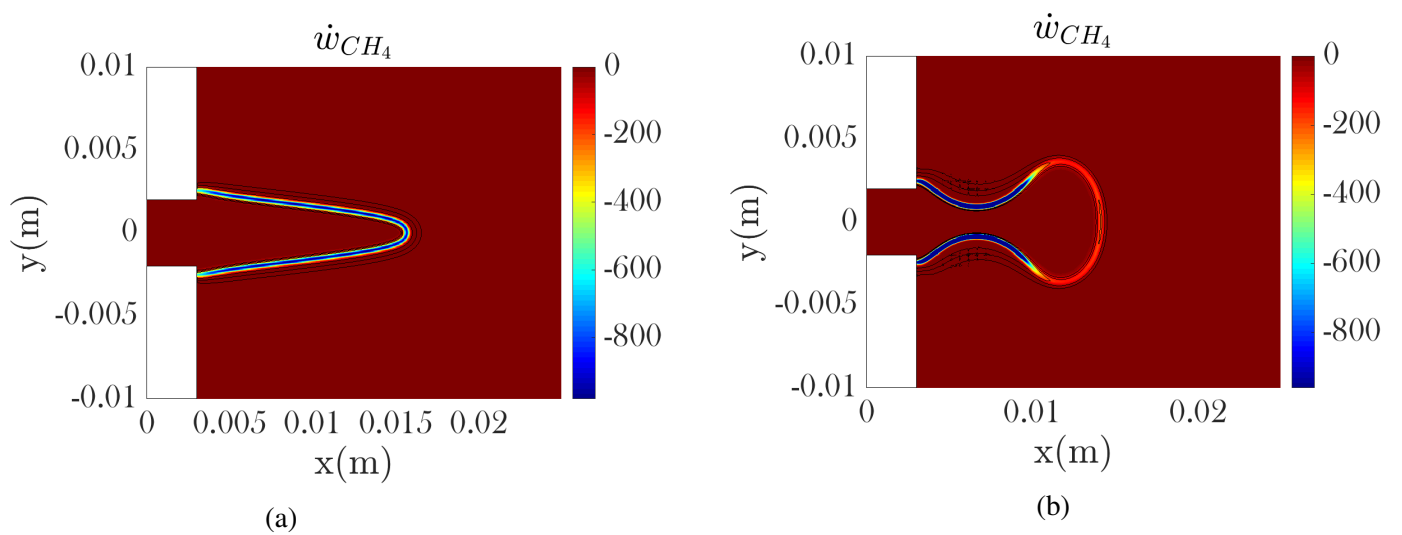


Figure 4.8: Volumetric molar production rate of CH_4 at (a)steady state and(b) For $\epsilon = 0.4$ case, with 270° phase at inlet.

CHAPTER 4. PERTURBED CASES

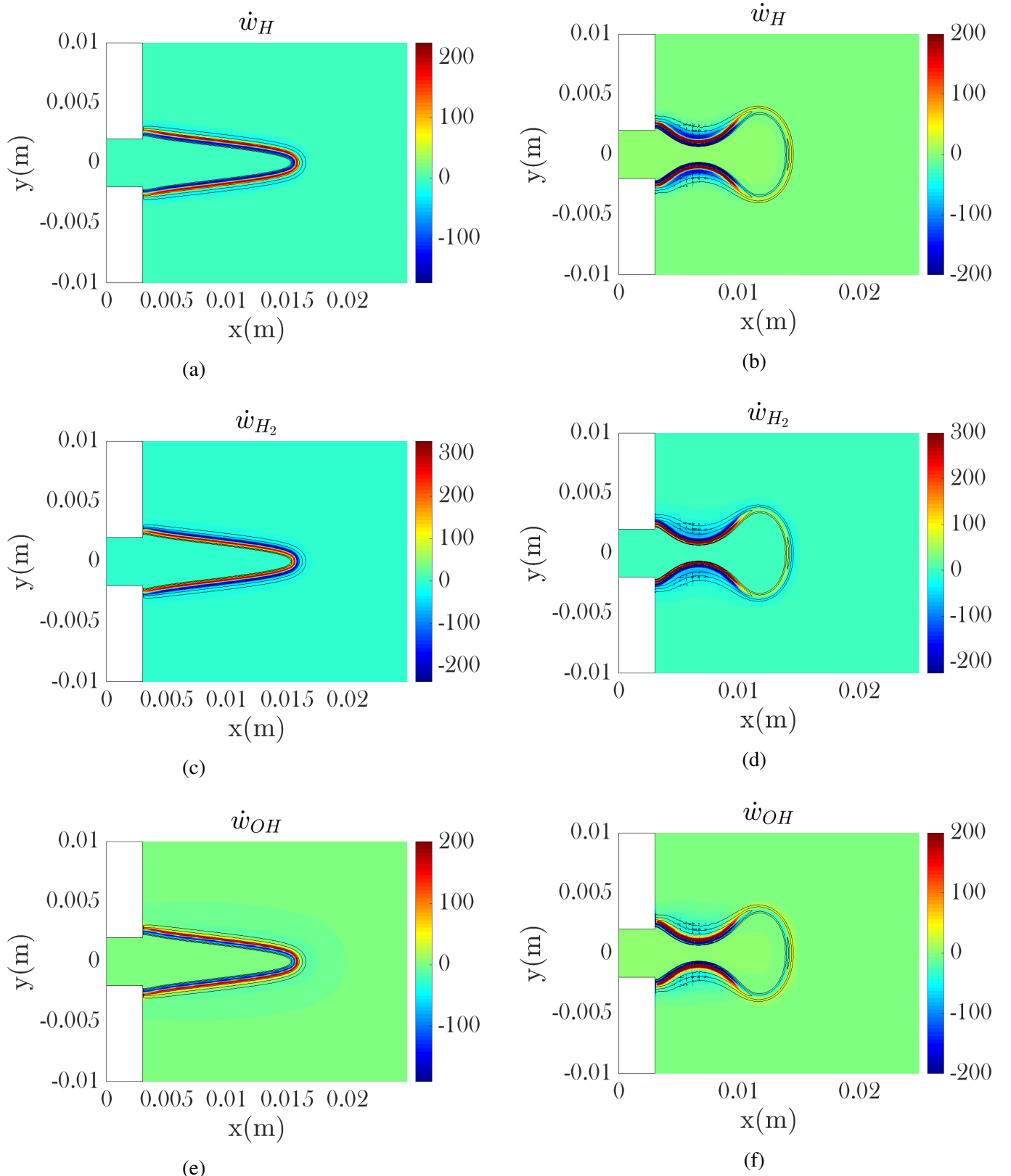


Figure 4.9: Volumetric molar production rate of H , H_2 and OH . (a),(c),(e) show steady state and (b),(d),(f) show $\epsilon = 0.4$ case, with 270° phase shift at inlet.

CHAPTER 4. PERTURBED CASES

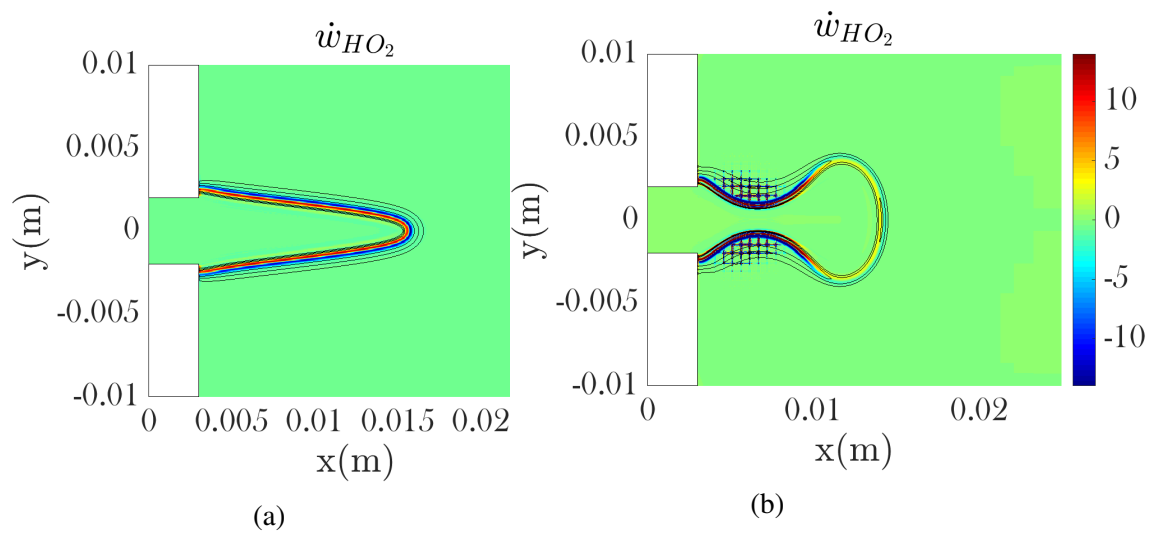


Figure 4.10: Volumetric molar production rate of HO_2 at (a) steady state and (b) For $\epsilon = 0.4$ case, with 270° phase at inlet.

Chapter 5

Conclusion

In the present work, we study slot stabilized flame without equivalence ratio perturbation and with three normalized perturbation amplitudes $\epsilon = 0.05, 0.2, 0.4$ is studied.

Analysis of steady state results without equivalence ratio perturbation is carried out to find local flame speed, flame curvature, and strain rate at 350K contour. From this, effects of curvature and strain rate on local flame speed are studied. Flame speeds are calculated for zero curvature and zero strain rate. It is found that they are in close agreement with standard flame speed. Also, from flame speed and strain rate plot, markstain's length is computed.

In analysis for perturbed case, each case is plotted with normalized minimum equivalence ratio extension below steady flammability limit and normalized frequency, to locate case either in flammable or non-flammable region. Case with $\epsilon = 0.05$ lie in flammable region where $\epsilon = 0.2$ and 0.4 lies in non-flammable region. But, no extinction is found out in any of the cases. In order to understand this flame behaviour, combined effect of strain rate and curvature on flammability limit needs to be considered which can be taken as future work.

Bibliography

- [1] Gaurav Bansal and Hong G. Im. Time scales in unsteady premixed flame extinction with composition fluctuations. *Combustion and Flame*, 150(4):404 – 408, 2007. ISSN 0010-2180. doi: <http://dx.doi.org/10.1016/j.combustflame.2007.06.005>. URL <http://www.sciencedirect.com/science/article/pii/S0010218007001575>. ii, 2, 3
- [2] A.L. Birbaud, S. Ducruix, D. Durox, and S. Candel. The nonlinear response of inverted v flames to equivalence ratio nonuniformities. *Combustion and Flame*, 154(3):356 – 367, 2008. ISSN 0010-2180. doi: <http://dx.doi.org/10.1016/j.combustflame.2008.05.017>. URL <http://www.sciencedirect.com/science/article/pii/S0010218008001855>. 5
- [3] David G. Goodwin, Harry K. Moffat, and Raymond L. Speth. Cantera: An object-oriented software toolkit for chemical kinetics, thermodynamics, and transport processes. <http://www.cantera.org>, 2017. Version 2.3.0. 9, 17
- [4] Evatt R Hawkes and Jacqueline H Chen. Direct numerical simulation of hydrogen-enriched lean premixed methane–air flames. *Combustion and Flame*, 138(3):242–258, 2004. 7
- [5] U.Maas J.Warnatz and R.W.Dibble. combustion (3rd edition). 7
- [6] Joseph Mathew, Richard Lechner, Holger Foysi, Joern Sesterhenn, and Rainer Friedrich. An Explicit Filtering Method for Large Eddy Simulation of Compressible Flows. *Phys. Fluids*, 15(8):2279–2289, 2003. ISSN 10706631. doi: 10.1063/1.1586271. 7

BIBLIOGRAPHY

- [7] Bonnie J McBride, Sanford Gordon, and Martin A Reno. Coefficients for calculating thermodynamic and transport properties of individual species. 1993. [7](#)
- [8] T J& Poinsot and SK Lele. Boundary conditions for direct simulations of compressible viscous flows. *Journal of computational physics*, 101(1):104–129, 1992. [8](#), [10](#)
- [9] Thierry Poinsot and Denis Veynante. *Theoretical and numerical combustion*. RT Edwards, Inc., 2005. [7](#), [17](#)
- [10] Kiran R. Study of transport and kinetic model for methane. *M.E. Thesis,IISc*, 2016. [4](#)
- [11] Ramanan Sankaran and Hong G Im. Dynamic flammability limits of methane/air premixed flames with mixture composition fluctuations. *Proceedings of the Combustion Institute*, 29(1):77–84, 2002. [ii](#), [2](#), [28](#), [30](#)
- [12] Shreekrishna, Santosh Hemchandra, and Tim Lieuwen. Premixed flame response to equivalence ratio perturbations. *Combustion Theory and Modelling*, 14(5):681–714, 2010. [v](#), [5](#)
- [13] C.J Sung, C.K Law, and J.-Y Chen. Augmented reduced mechanisms for no emission in methane oxidation. *Combustion and Flame*, 125(1):906 – 919, 2001. ISSN 0010-2180. doi: [http://dx.doi.org/10.1016/S0010-2180\(00\)00248-0](http://dx.doi.org/10.1016/S0010-2180(00)00248-0). URL <http://www.sciencedirect.com/science/article/pii/S0010218000002480>. [4](#)
- [14] T.Velayutham. Direct numerical simulation of compressible round jets. *Thesis IISc*, year=2015,. [8](#)
- [15] Emilien Varea, Vincent Modica, Alexis Vandel, and Bruno Renou. Measurement of laminar burning velocity and markstein length relative to fresh gases using a new postprocessing procedure: Application to laminar spherical flames for methane, ethanol and isooc-tane/air mixtures. *Combustion and Flame*, 159(2):577 – 590, 2012. ISSN 0010-2180. doi: <http://dx.doi.org/10.1016/j.combustflame.2011.09.002>. URL <http://www.sciencedirect.com/science/article/pii/S001021801100277X>. [vi](#), [18](#), [21](#)

BIBLIOGRAPHY

- [16] C. R. Wilke. A viscosity equation for gas mixtures. *The Journal of Chemical Physics*, 18(4): 517–519, 1950. doi: 10.1063/1.1747673. URL <http://dx.doi.org/10.1063/1.1747673>.
7
- [17] Ren Wu and Santosh Hemchandra. Premixed flame response to equivalence ratio perturbations:lean flammability cross-over. *7th US National Technical Meeting of the combustion institute Hosted by the Georgia Institute of Technology, Atlanta GA*, March 20-23, 2011. 3